aerospace

MDPI

Article

Experimental Evaluation of Fatigue Strength of AlSi10Mg Lattice Structures Fabricated by AM

Carlo Giovanni Ferro *, Sara Varetti and Paolo Maggiore

Department of Mechanical Engineering and Aerospace (DIMEAS), Polytechnic University of Turin, 10129 Turin, Italy
* Correspondence: carlo.ferro@polito.it; Tel.: +39-011-090-6850

Abstract: There is evidence that Additive Manufacturing (AM) plays a crucial role in the fourth industrial revolution. The design freedom provided by this technology is disrupting limits and rules from the past, enabling engineers to produce new products that are otherwise unfeasible. Recent developments in the field of Selective Laser Melting (SLM) have led to a renewed interest in lattice structures that can be produced non-stochastically in previously unfeasible dimensional scales. One of the primary applications is aerospace engineering where the need for light weights and performance is urgent to reduce the carbon footprint of civil transport around the globe. Of particular concern is fatigue strength. Being able to predict fatigue life in both LCF (Low Cycle Fatigue) and HCF (High Cycle Fatigue) is crucial for a safe and reliable design in aerospace systems and structures. In the present work, an experimental evaluation of compressive–compressive fatigue behavior has been performed to evaluate the fatigue curves of different cells, varying sizes and relative densities. A Design of Experiment (DOE) approach has been adopted in order to maximize the information extractable in a reliable form.

Keywords: additive manufacturing; lattice structures; fatigue strength; trabecular structures

Citation: Ferro, C.G.; Varetti, S.; Maggiore, P. Experimental Evaluation of Fatigue Strength of AlSi10Mg Lattice Structures Fabricated by AM. *Aerospace* **2023**, *10*, 400. https://doi.org/10.3390/aerospace10050400

Academic Editor: Andrea Di Schino

Received: 8 March 2023
Revised: 28 March 2023
Accepted: 21 April 2023
Published: 25 April 2023

1. Introduction

Additive Manufacturing (AM) has emerged as a game-changer in the field of aerospace engineering, providing new opportunities for the design and manufacture of complex structures and systems with improved thermo-mechanical properties [1–5]. Currently, one of the key challenges in aerospace engineering is the development of low power effective anti-ice systems, which are essential for ensuring safe and efficient operations in cold and icy conditions [6–8]. State-of-the-art anti-icing systems use hot air spilled from the turbine engine compressors [9]. These systems present low thermal efficiencies and high losses [10–13]. In recent years, lattice structures made of AlSi10Mg alloy have emerged as a promising candidate for the development of innovative anti-ice systems [14–16]. Lattice structures indeed present interesting thermal and mechanical properties for heat and structure components making them the ideal candidate for a novel anti-icing material to integrate into the leading edge structure (Figure 1). The emerging benefit could be a sensible reduction of the air spilled and therefore, a reduction of the fuel consumption. Unfortunately, lattice structures in the core of the sandwich panel are subjected to cyclic loads. Being able to predict the fatigue strength under cyclic loading is currently one of the greatest challenges [17,18]. A search of the literature revealed a few studies, which experimentally evaluated the fatigue curves of lattice structures made of AlSi10Mg fabricated by AM [19,20]. In order to fill the gap between the requirements for a safe design of a critical component and the available literature, an extensive analysis campaign has been developed. This paper presents results aimed at investigating the fatigue strength of lattice structures made of AlSi10Mg alloy fabricated by AM in order to provides insights into the design of innovative systems for aerospace applications [21].

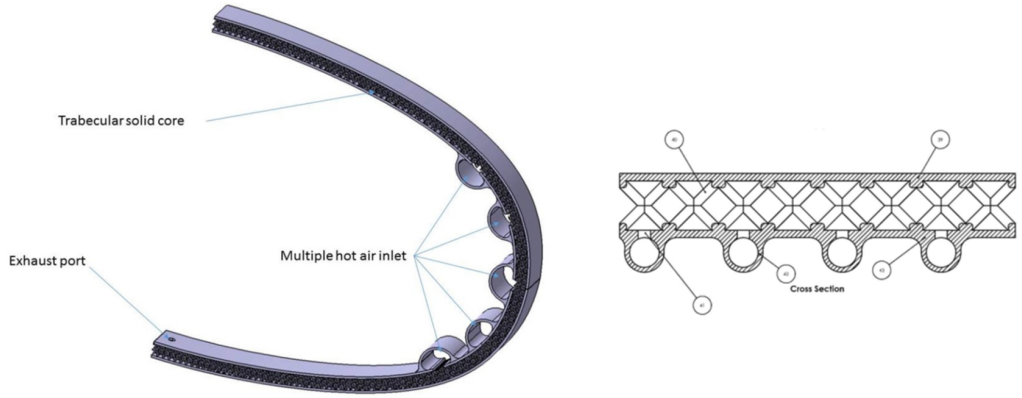

(**a**) (**b**)

Figure 1. Integrated Anti-Ice Panel. (**a**): Isometrical View of the proposed novel anti-ice panel (**b**): Cross Section of the patented solutions.

Fatigue strength is a crucial parameter in the design of aerospace components, especially those that are subjected to cyclic loading. Lattice structures, also known as cellular or honeycomb structures, are highly desirable due to their lightweight nature and high stiffness-to-weight ratio [22–24]. They have been used in various applications, including heat exchangers, sandwich panels, and energy absorption systems [25–28]. AlSi10Mg is an aluminum alloy that has been extensively used in AM due to its excellent mechanical properties and good weldability [29]. In the case of anti-ice systems, lattice structures made of AlSi10Mg have been proposed as a potential solution due to their ability to provide excellent anti-ice performance by allowing a continuous flow of hot air to pass through the structure, thus melting the ice on its surface [21,30]. However, the fatigue strength of these structures is not well understood, which poses a significant challenge in their design and optimization. The experimental study presented in this paper involved the testing of AlSi10Mg lattices fabricated by AM under cyclic loading to determine their fatigue limits. The results of this study will provide new insights into the behavior of these structures under cyclic loading and will help in understanding their failure mechanisms. The findings will also aid in the development of design guidelines for lattice structures and will enable the optimization of innovative anti-ice systems for aerospace applications [31]. In summary, the experimental evaluation of the fatigue strength of lattice structures is of strong significant interest to the aerospace industry.

2. Materials and Methods

2.1. Design of Experiment (DOE)

The fatigue tests on trabecular lattices had the primary objective to experimentally characterize the fatigue life curve of different types of non-stochastic foams built with AlSi10Mg by AM. The data for this study were collected using a DOE approach [32] in order to provide novel information regarding the effects of design parameters (cell type, cell size and relative density) on lattice fatigue performance [33]. Although some research has been carried out on fatigue with this approach [33], none of the previous studies have reported such a wide investigation for AlSi10Mg.

Three different trusses layout have been selected: Body-Centered Cubic with vertical beams (Bccz), Octet and Rhombic Dodecahedron. For each cell type, two cells sizes, 5 mm and 7 mm, were adopted with two relative densities: 25% and 30%. In order to limit the number of specimens and the cost of the experimental campaign, the DOE with three factors and hybrid levels for each factor was executed in fractional factorial form. The details of the specimens produced for the fatigue test are reported in Table 1.

Table 1. Factors selected to design specimens for fatigue tests.

Cell Type	Cell Size [mm]	Relative Density [%]
Bccz	5	25
Bccz	5	30
Bccz	7	30
Rhombic Dodecahedron	5	25
Rhombic Dodecahedron	5	30
Rhombic Dodecahedron	7	30
Octet Truss	5	25
Octet Truss	5	30
Octet Truss	7	30

2.2. Specimen Design

The trabecular specimens presented a height/base side ratio of 2:1, similar to the one proposed previously [7]. Each specimen had a square bottom and a longer height to prevent the effect of borders and specimen shape. A picture of Bccz is shown in Figure 2 while detailed drawings with dimensions are reported in Appendix C. All specimens have two flat skins 1 mm thick at the square bases. This skin has been added in order to uniformly distribute the stress on first layer cells and to avoid peaks caused by manufacturing imperfections.

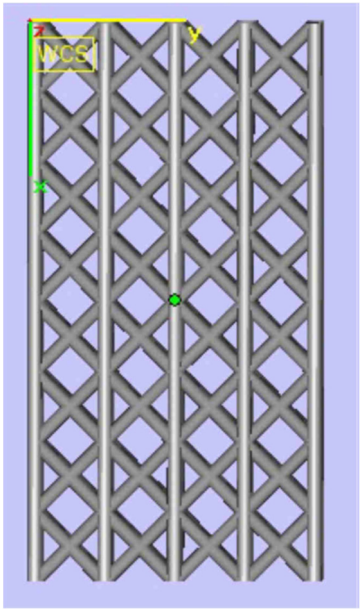

Figure 2. CAD Design of a Specimen.

2.3. Fatigue Test Setup

Compression–compression fatigue tests were carried out according to protocols in the scientific literature [34–37].

A variable maximum load of 80%, 60%, 40% and 20% of the static yield (σ_{02} calculated according to ASTM E9) was imposed in order to obtain the Wohler curves. The ratio parameter of $R = 0.1$ implies that the compressive load on the specimens oscillates with a sinusoidal from 10% to 100% of the imposed load with a frequency speed of 50 cyclic loads per second (50 Hz).

The maximum value of the compression is defined as σ_M and can be obtained from Equation (1); the parameter x corresponds to a linear multiplying value of 80%, 60%, 40% and 20%; σ_{02} is the average yield load of the static uniaxial compression tests on the corresponding trabecular specimens. This value has been separately calculated by previous experimental static compressive test on analogous specimens [38].

The minimum value of the compression is reported as σ_m, obtained from Equation (2), where the R parameter is maintained equal to 0.1. The median value between σ_M and σ_m is σ_a, calculated using Equation (3). In order to evaluate the Wohler curve, it is then necessary to record the Number of cycles (N) corresponding to the specimen failure. The imposed upper limit for the cycles is N equal to 1.5×10^7, suitable for airframe structures and the systems safe-life approach [39].

$$\sigma_M = x\sigma_{02} \tag{1}$$

$$\sigma_m = R\sigma_M \tag{2}$$

$$\sigma_a = (\sigma_M - \sigma_m)/2 \tag{3}$$

The values of σ_M, σ_m, σ_a and N are tabulated in Appendix A. All the specimens, three for each type, were processed with an Instron machine. The test machine setup has been prepared with a flat attachment, a load cell of 50 kN and a constant displacement of 1 mm/min, as shown in Figure 3.

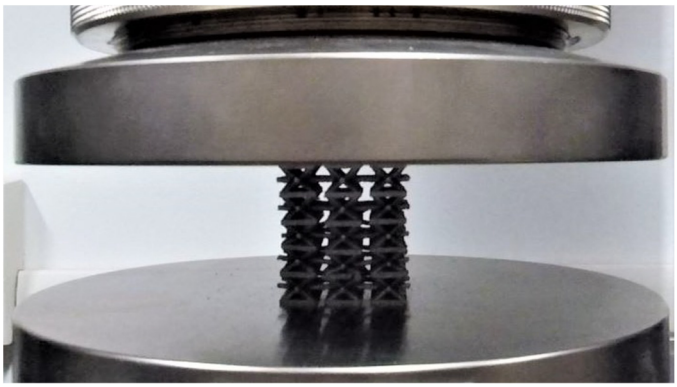

Figure 3. Testing Machine Setup.

The same AlSi10Mg material as [7] was used. The specimen's size was maintained as much as possible to be coherent to the 20 mm × 20 mm × 40 mm proposed in [7] in order to preserve the comparability of the data.

3. Results

In this section, the results obtained from the fatigue tests will be disclosed. All the numerical evidence are reported in Appendix A subdivided by cell type. For each cell type, Wohler curves will be provided and discussed. The Wohler curves relate the amplitude of the load, σ_a, for each sample and the number of cycles at which the specimen breakdown occurs. Subsequently, images of broken specimens will be shown to provide insights on the failure mechanism.

3.1. Rhombic Dodecahedron

The graph in Figure 4. reports the Wohler curves for all the rhombic specimens tested. At equal σ_a (load amplitude), the greatest fatigue life was that of specimens with a smaller cell size, 5 mm, and higher density, 30%. The second longest endurance was produced by cells with a 7 mm cell size and 30% relative density. The lowest fatigue life was witnessed from specimens with a 5 mm cell size and 25% relative density. The most relevant aspect of this graph was the effect of cell size. Increasing cell size, while maintaining fixed the relative density of the specimen (i.e., same amount material per cubic centimeter), noticeably reduced the fatigue life as reported by the comparison between 7_30 and 5_30 cells.

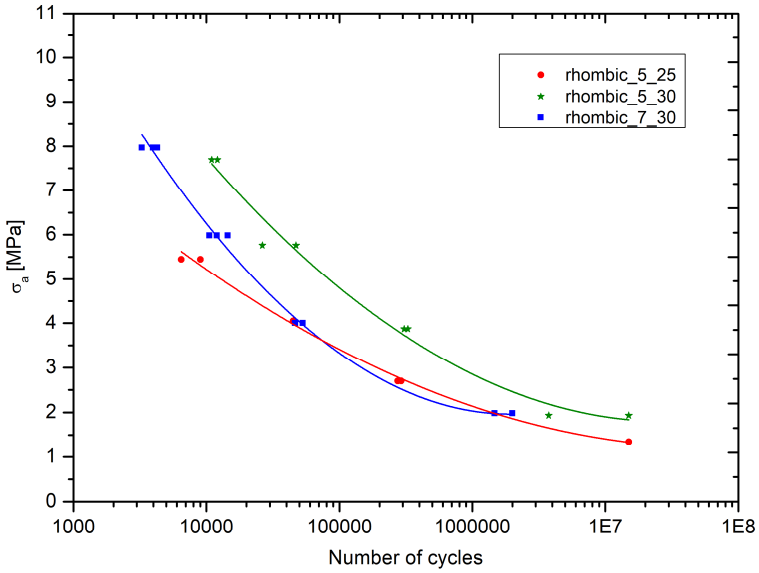

Figure 4. Wohler curves for rhombic dodecahedron specimens.

The effect of relative density was less stable in all the tested stress amplitudes. As reported in Appendix B, in the main effect graph in Figure A1, the effect of the relative density was not monotonous. While at higher loads the increase of the relative density seemed to provide a higher fatigue life, this was not true for lower loads (60% and 20% of the yield stress). This aspect will require further dedicated analysis in the future.

The photos of the rhombic specimens before the fatigue test are shown in Figures 5 and 6. while pictures of specimens after the test are shown in Figure 6.

The failure occurred along a 45° plane with respect to the *Z*-axis and started from a corner of the specimen. The deformation evidenced before the failure was almost absent; the connections broke internally one by one along the plane until the resistant section became insufficient and caused the collapse of the specimen. From the images, it was possible to observe that the breaking of the specimens subjected to higher loads (80% and 60% of σ_{02}) was clearer and more similar to the one from the static compression tests. On the other hand, the rupture of the specimens subjected to lower loads (40% and 20% of σ_{02}) was more irregular and acted through several fractures' planes simultaneously, causing the final separation of the specimen into more than two pieces. This difference was particularly marked for the 7 mm cells, as visible in Figure 6. For cells with a lower relative density, such as 5-25, irregular fractures were already present for higher loads, such as 60% of σ_{02}.

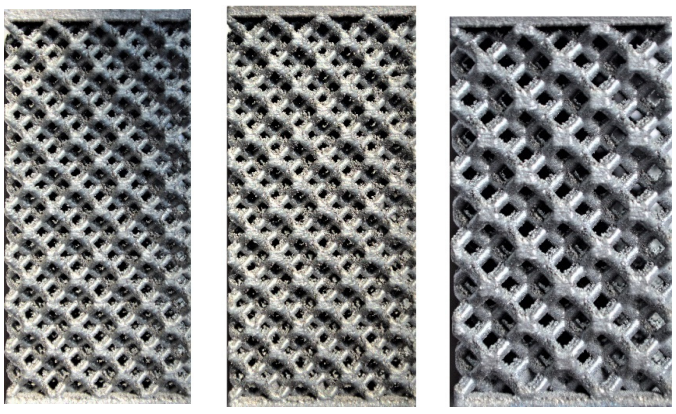

(**a**) (**b**) (**c**)

Figure 5. Lateral view of the Rhombic dodecahedron AlSi10Mg specimens for fatigue test: (**a**) Rhom-5-25, (**b**) Rhom-5-30 and (**c**) Rhom-7-30.

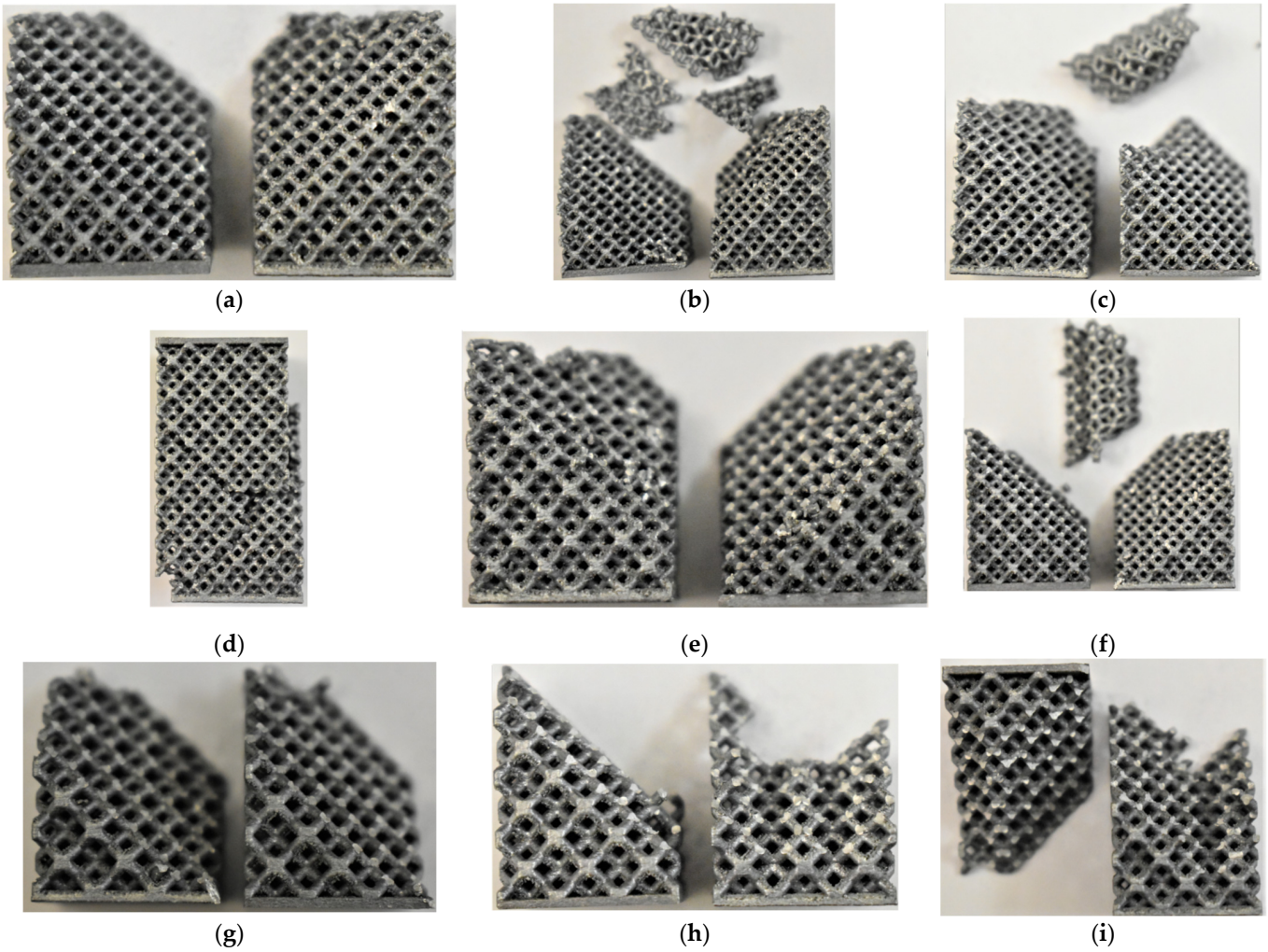

Figure 6. Rhombic cells subjected to fatigue test: (**a**) cell size 5 mm, relative density 25%, max load 80% σ_{02}; (**b**) cell size 5 mm, relative density 25%, max load 60% σ_{02}; (**c**) cell size 5 mm, relative density 25%, max load 40% σ_{02}; (**d**) cell size 5 mm, relative density 30%, max load 80% σ_{02}; (**e**) cell size, 5 mm relative density 30%, max load 60% σ_{02}; (**f**) cell size 5 mm, relative density 30%, max load 40% σ_{02}; (**g**) cell size 7 mm, relative density 30%, max load 80% σ_{02}; (**h**) cell size 7 mm, relative density 30%, max load 60% σ_{02}; (**i**) cell size 7 mm, relative density 30%, max load 40% σ_{02}.

3.2. Octet Truss

The graph in Figure 7 reports the Wohler curves for all the tested Octet truss specimens. In accordance with the present results, the longest fatigue life was shown by the 5-30 specimens, followed by the specimens 7-30 and 5-25 with intersecting behaviors.

Similar to the case with Rhombic cells, Octet truss curves for 5-30 and 7-30 were almost parallel to each other, with the 7-30 case shifted to lower cycles. This behavior suggests a clear negative effect of increasing of the cell size with same relative density.

As for the 7-30 vs. 5-25 trend, relative density played a beneficial effect at higher loads (80% and 60% of σ_{02}) and reported a dissimilar trend at lower loads (40% and 20% of yield stress). Additionally, in this scenario, further analyses are required to deeply investigate the effect of this parameter. It is important to note that specimens 5-30 and 5-25 reached the imposed fatigue limit (1.5×10^7 cycles) without breaking with a σ_M equal to the 20% of yield stress.

The photos of the Octet specimens before the fatigue test are reported in Figure 8 while pictures of specimens after the test are in Figure 9.

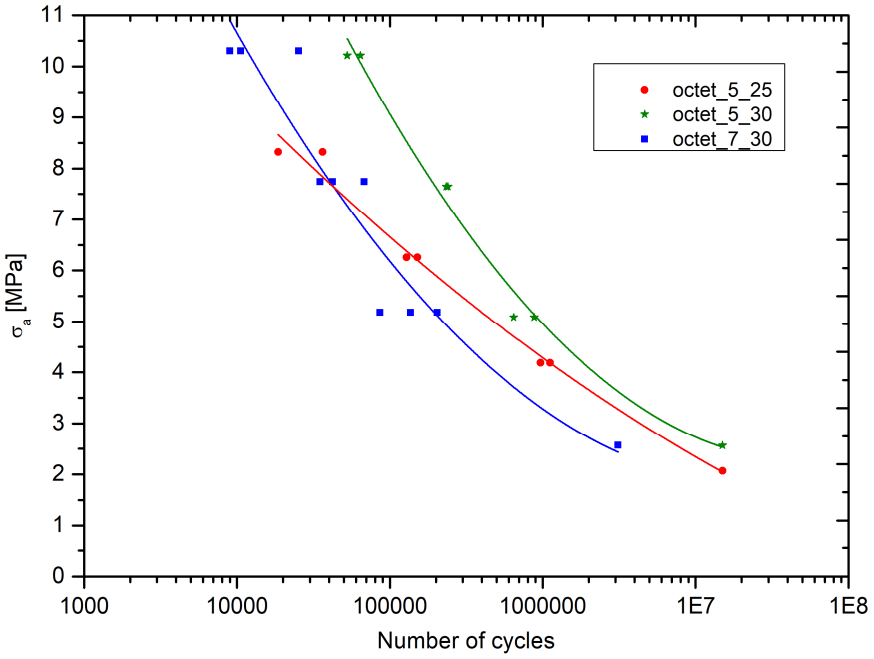

Figure 7. Wohler curves for Octet truss specimens.

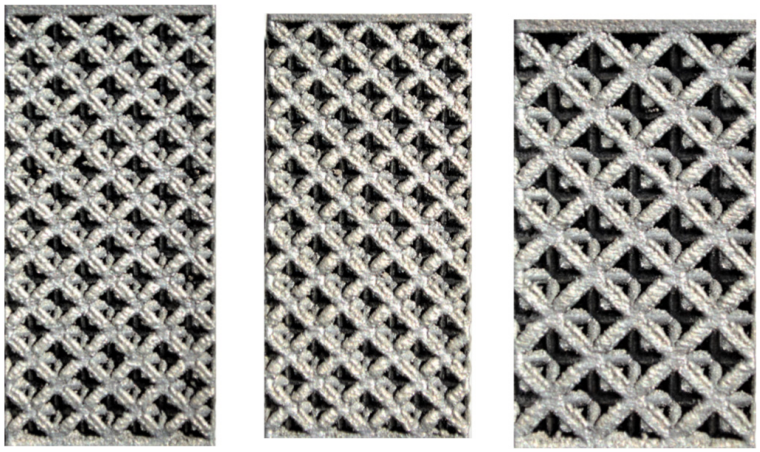

Figure 8. Lateral view of the Octet truss AlSi10Mg specimens for fatigue test: (**a**) Octet truss 5-25, (**b**) Octet truss 5-30 and (**c**) Octet truss 7-30.

The fracture of the specimen was, in part, similar to that evidenced during compression tests. The failure occurred along a 45° plane with respect to the *Z*-axis and started from a corner of the specimen. Deformation before the failure was almost absent; the connections broke internally one by one along the plane until the resistant section became insufficient and caused the collapse of the specimen. The failure mode of the 5-25 specimens subjected to all loads was more irregular compared to the others and acted simultaneously on several planes causing the final separation of the specimen into more than two pieces. Similarly, the 7-30 specimens subjected to higher loads (80% and 60% of σ_{02}) also failed in a similar manner to that seen for the compression tests; on the other hand, the failure mode of the same cells when subjected to lower loads (40% and 20% of σ_{02}) was more irregular and acted on several planes simultaneously, causing final separation of the specimen into more than two pieces.

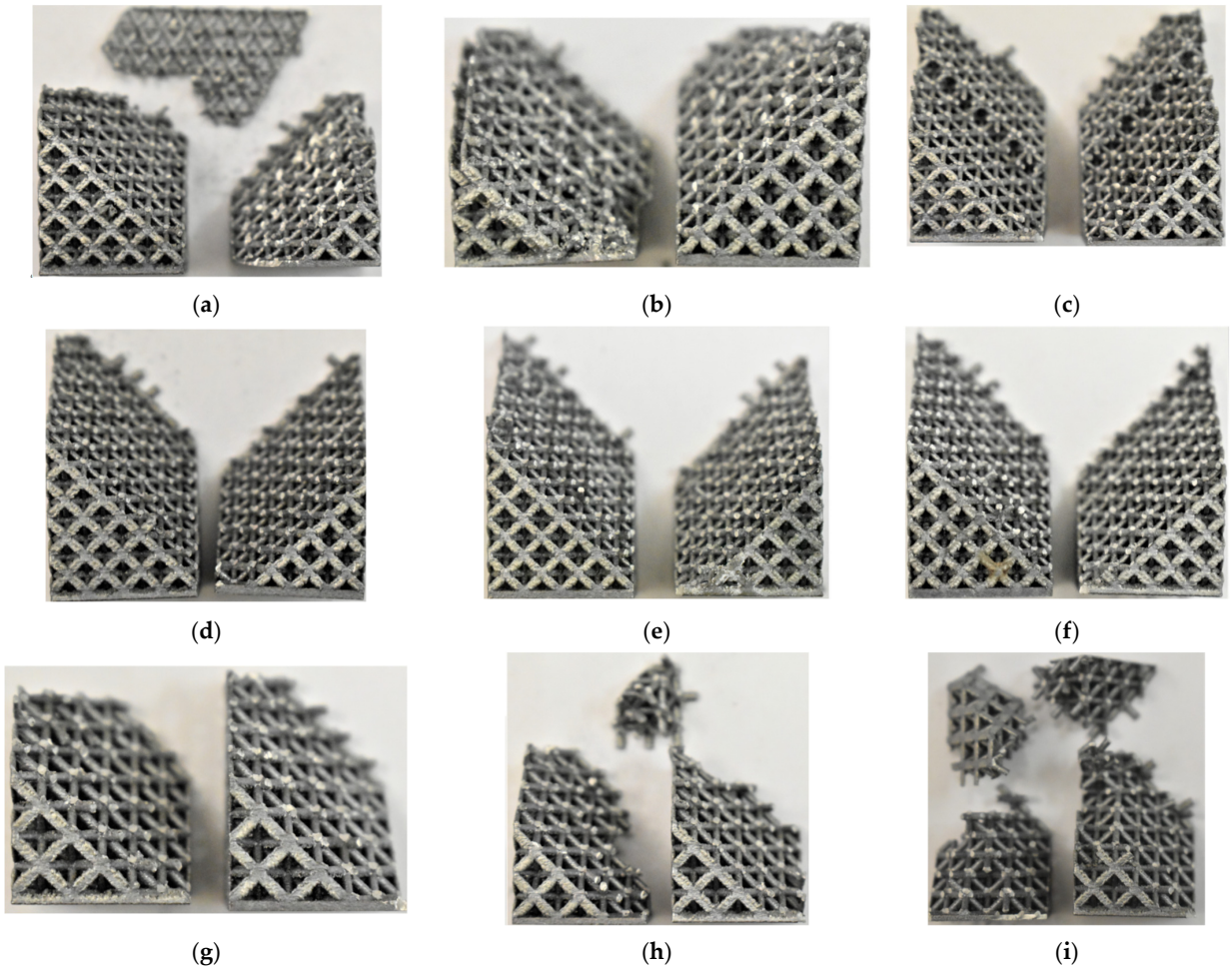

Figure 9. Octet cells subjected to fatigue: (**a**) cell size 5 mm, relative density 25%, max load 80% σ_{02}; (**b**) cell size 5 mm, relative density 25%, max load 60% σ_{02}; (**c**) cell size 5 mm, relative density 25%, max load 40% σ_{02}; (**d**) cell size 5 mm, relative density 30%, max load 80% σ_{02}; (**e**) cell size 5 mm, relative density 30%, max load 60% σ_{02}; (**f**) cell size 5 mm, relative density 30%, max load 40% σ_{02}; (**g**) cell size 7 mm, relative density 30%, max load 80% σ_{02}; (**h**) cell size 7 mm, relative density 30%, max load 60% σ_{02}; (**i**) cell size 7 mm, relative density 30%, max load 40% σ_{02}.

3.3. Bccz

The fatigue Wohler curves for the Bccz specimens, presented in Figure 10, remained partially completed due to the different resistance behaviors found. The specimens already reached the preset limit of 1.5×10^7 cycles at 60% of the load for the 5 mm cells and 40% for the 7 mm cells; for this reason, it was impossible to obtain complete Wohler curves. Further improvements will enhance the span of loads tested by introducing a setup to produce between 80% and 100% of the yield load. The greatest fatigue resistance of the Bccz specimens was given by the vertical struts. During the static compression tests, the vertical struts deformed and then broke with buckling-like deformation. The photos of the Bccz specimens before the fatigue test are shown Figure 11 while pictures of specimens after the test are shown in Figure 12.

In the fatigue tests, the imposed load was not sufficient to reach the buckling limit for the vertical struts. As visible in Figure 12, the failure of the specimen, when it occurs, was due to the breaking of the struts at the central nodes, as seen for Rhombic and Octet cells. The fracture then followed the plane at 45° only in some points, but in most cases, there was a sparse and irregular separation of the cells. Further analysis will be dedicated to a higher σ_M.

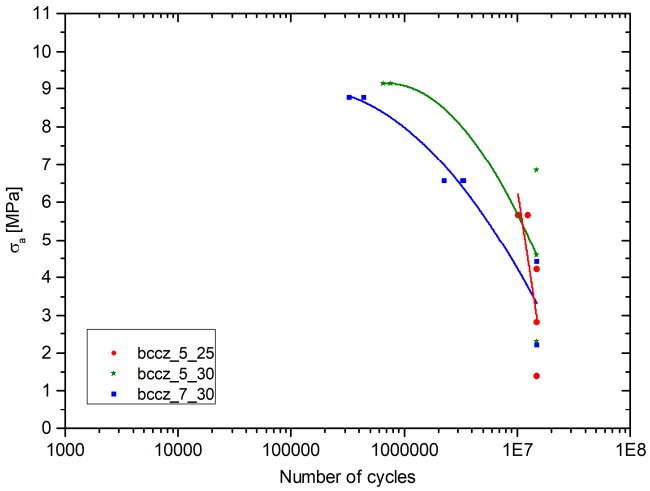

Figure 10. Wohler curves for Bccz specimens.

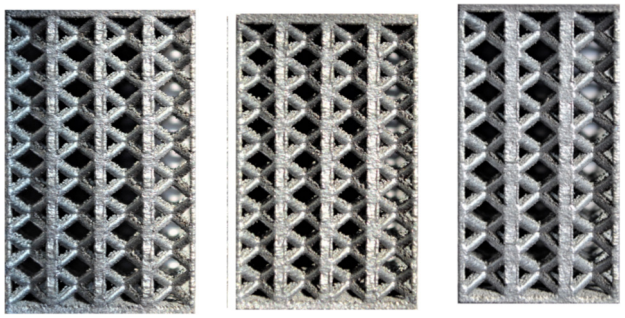

(**a**) (**b**) (**c**)

Figure 11. Lateral view of the Bccz AlSi10Mg specimens for fatigue test: (**a**) Bccz 5-25, (**b**) Bccz 5-30 and (**c**) Bccz 7-30.

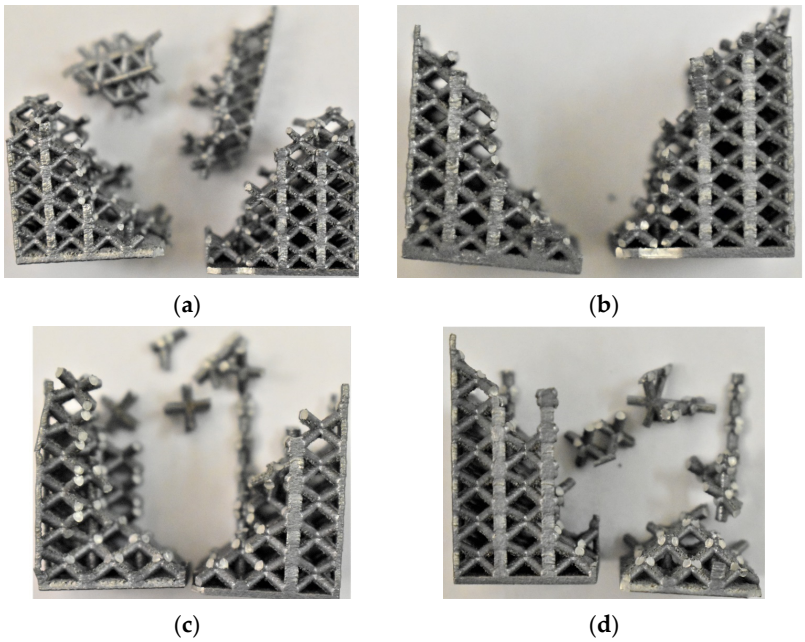

(**a**) (**b**)

(**c**) (**d**)

Figure 12. Bccz cells subjected to fatigue: (**a**) cell size 5 mm, relative density 25%, max load 80% σ_{02}; (**b**) cell size 5 mm, relative density 30%, max load 80% σ_{02}; (**c**) cell size 7 mm, relative density 30%, max load 80% σ_{02}; (**d**) cell size 7 mm, relative density 30%, max load 60% σ_{02}.

4. Discussion

Several reports have shown that different cell topologies provide different fatigue life behaviors [40,41]. This section will provide a comparison of the three architected cells subjected to the same load path.

What is striking about the graphs reported in Figure 13 is the homogeneous trend. Bccz cells, as commented above, always performed better, followed by Octet cells and Rhombic cells. The last two cells' topologies presented similar curves, which showed different trends than that of the Bccz cells. A possible explanation for this might be that Rhombic and Octet cells are bending-dominated cells [42] while Bccz cells are stretch-dominated cells that benefit enormously when the compression load on the vertical cells does not reach the buckling limit.

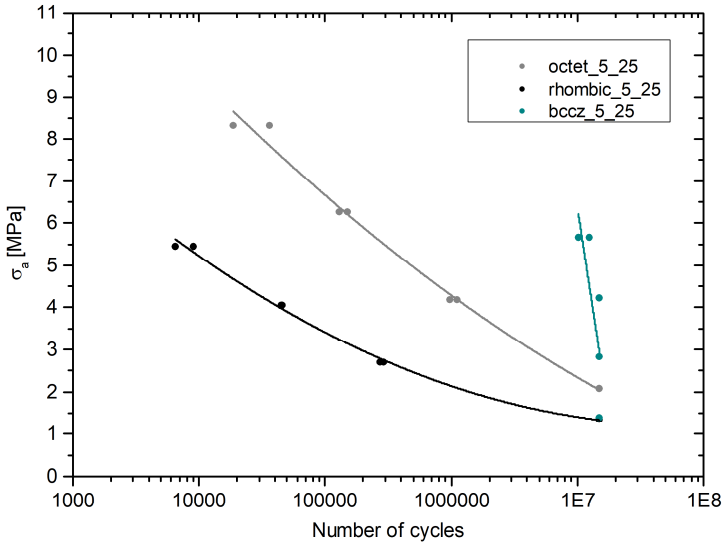

(**a**)

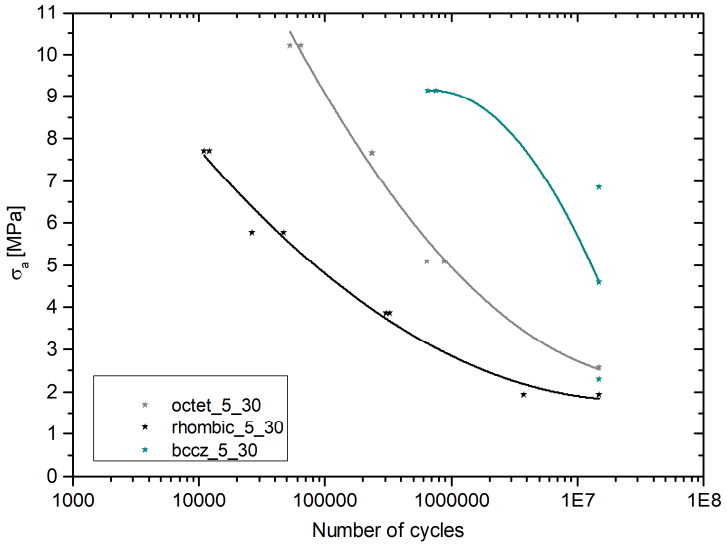

(**b**)

Figure 13. *Cont.*

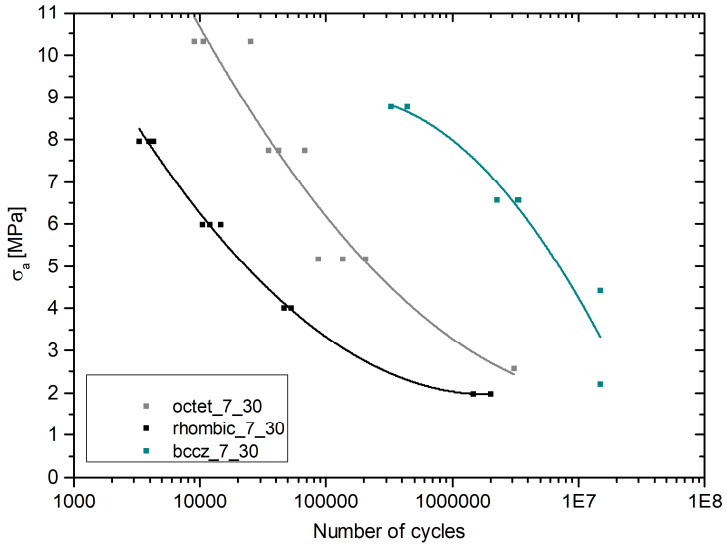

(**c**)

Figure 13. Wohler curves: (**a**) cell size 5 mm and 25% relative density; (**b**) cell size 5 mm and 30% relative density; (**c**) cell size 7 mm and 30% relative density.

The results provided are significant in at least two major respects. Firstly, they provide reliable encouraging data on the fatigue life of different cells with various cell sizes and different relative densities. Secondly, they establish some useful correlations between design parameters and fatigue life.

Despite these promising results, further work is still required to establish the real fatigue limit of Bccz cells and deeply evaluate the effect of relative density on the fatigue performance for bending-dominated cells type.

5. Conclusions

Wohler fatigue curves for different types of trabecular structures have been evaluated for the first time. This study has identified clear trends and correlations for the cell type and cell size effects on the number of cycles at rupture during compression–compression fatigue. Further investigations are needed to deepen our understanding of some nonlinear phenomena on the effect of the relative density. Overall, this study has strengthened the idea that lattice structures are a valid resource for aerospace structures due to their light weight and their high specific structural performances. In spite of its limitations, this study certainly adds important novel findings to aid our understanding of fatigue life prediction.

6. Patents

In this paper, research on the fatigue life of trabecular structures was performed. This work is part of effort towards a patent for a novel anti-icing system for aircraft use [8].

Author Contributions: Conceptualization, C.G.F.; methodology, C.G.F.; software, C.G.F. and S.V.; validation, C.G.F. and S.V.; formal analysis, C.G.F. and S.V.; investigation, C.G.F. and S.V.; resources, P.M.; data curation, S.V.; writing—original draft preparation, C.G.F.; writing—review and editing, S.V.; visualization, P.M.; supervision, P.M.; project administration, P.M.; funding acquisition, P.M. All authors have read and agreed to the published version of the manuscript.

Funding: This research received no external funding.

Data Availability Statement: Data are already all disclosed in Appendices A–C.

Conflicts of Interest: The authors declare no conflict of interest.

Appendix A

AlSi10Mg specimens for fatigue test with Bccz cell. The identification code of the specimens is: Celle shape-Cell size-Solid volume fraction (nominal)-Serial number.

Table A1. BCC-Z Fatigue Results.

Id Code	σ_M [MPa]	σ_m [MPa]	σ_a [MPa]	N
Bccz-5-25-1	12.6	1.26	5.67	10,178,091
Bccz-5-25-2	12.6	1.26	5.67	12,441,038
Bccz-5-25-3	12.6	1.26	5.67	-
Bccz-5-25-4	9.4	0.94	4.23	>15,000,000
Bccz-5-25-5	9.4	0.94	4.23	>15,000,000
Bccz-5-25-6	9.4	0.94	4.23	-
Bccz-5-25-7	6.3	0.63	2.84	>15,000,000
Bccz-5-25-8	6.3	0.63	2.84	>15,000,000
Bccz-5-25-9	6.3	0.63	2.84	-
Bccz-5-25-10	3.1	0.31	1.40	>15,000,000
Bccz-5-25-11	3.1	0.31	1.40	>15,000,000
Bccz-5-25-12	3.1	0.31	1.40	-
Bccz-5-30-1	20.3	2.03	9.14	654,563
Bccz-5-30-2	20.3	2.03	9.14	762,810
Bccz-5-30-3	20.3	2.03	9.14	-
Bccz-5-30-4	15.2	1.52	6.84	>15,000,000
Bccz-5-30-5	15.2	1.52	6.84	>15,000,000
Bccz-5-30-6	15.2	1.52	6.84	-
Bccz-5-30-7	10.2	1.02	4.59	>15,000,000
Bccz-5-30-8	10.2	1.02	4.59	>15,000,000
Bccz-5-30-9	10.2	1.02	4.59	-
Bccz-5-30-10	5.1	0.51	2.30	>15,000,000
Bccz-5-30-11	5.1	0.51	2.30	>15,000,000
Bccz-5-30-12	5.1	0.51	2.30	-
Bccz-7-30-1	19.5	1.95	8.78	326,837
Bccz-7-30-2	19.5	1.95	8.78	440,166
Bccz-7-30-3	19.5	1.95	8.78	326,161
Bccz-7-30-4	14.6	1.46	6.57	3,362,847
Bccz-7-30-5	14.6	1.46	6.57	3,331,678
Bccz-7-30-6	14.6	1.46	6.57	2,249,586
Bccz-7-30-7	9.8	0.98	4.41	>15,000,000
Bccz-7-30-8	9.8	0.98	4.41	>15,000,000
Bccz-7-30-9	9.8	0.98	4.41	>15,000,000
Bccz-7-30-10	4.9	0.49	2.21	>15,000,000
Bccz-7-30-11	4.9	0.49	2.21	>15,000,000
Bccz-7-30-12	4.9	0.49	2.21	>15,000,000

AlSi10Mg specimens for fatigue test with Rhombic dodecahedron cell. The identification code of the specimens is: Cell shape-Cell size-Solid volume fraction (nominal)-Serial number.

Table A2. Rhombic Dodecahedron Fatigue Results.

Id Code	σ_M [MPa]	σ_m [MPa]	σ_a [MPa]	N
Rhom-5-25-1	12.1	1.21	5.45	9044
Rhom-5-25-2	12.1	1.21	5.45	6480
Rhom-5-25-3	12.1	1.21	5.45	-
Rhom-5-25-4	9	0.9	4.05	45,544
Rhom-5-25-5	9	0.9	4.05	45,031
Rhom-5-25-6	9	0.9	4.05	-
Rhom-5-25-7	6	0.6	2.70	291,522
Rhom-5-25-8	6	0.6	2.70	274,062
Rhom-5-25-9	6	0.6	2.70	-
Rhom-5-25-10	3	0.3	1.35	>15,000,000
Rhom-5-25-11	3	0.3	1.35	>15,000,000
Rhom-5-25-12	3	0.3	1.35	-
Rhom-5-30-1	17.1	1.71	7.70	12,100

Table A2. *Cont.*

Id Code	σ_M [MPa]	σ_m [MPa]	σ_a [MPa]	N
Rhom-5-30-2	17.1	1.71	7.70	10,947
Rhom-5-30-3	17.1	1.71	7.70	-
Rhom-5-30-4	12.8	1.28	5.76	47,132
Rhom-5-30-5	12.8	1.28	5.76	26,329
Rhom-5-30-6	12.8	1.28	5.76	-
Rhom-5-30-7	8.6	0.86	3.87	327,084
Rhom-5-30-8	8.6	0.86	3.87	307,454
Rhom-5-30-9	8.6	0.86	3.87	-
Rhom-5-30-10	4.3	0.43	1.94	>15,000,000
Rhom-5-30-11	4.3	0.43	1.94	3,755,825
Rhom-5-30-12	4.3	0.43	1.94	-
Rhom-7-30-1	17.7	1.77	7.97	4281
Rhom-7-30-2	17.7	1.77	7.97	3281
Rhom-7-30-3	17.7	1.77	7.97	3970
Rhom-7-30-4	13.3	1.33	5.99	14,484
Rhom-7-30-5	13.3	1.33	5.99	12,010
Rhom-7-30-6	13.3	1.33	5.99	10,550
Rhom-7-30-7	8.9	0.89	4.01	53,097
Rhom-7-30-8	8.9	0.89	4.01	46,449
Rhom-7-30-9	8.9	0.89	4.01	46,723
Rhom-7-30-10	4.4	0.44	1.98	1,471,143
Rhom-7-30-11	4.4	0.44	1.98	2,004,674
Rhom-7-30-12	4.4	0.44	1.98	-

AlSi10Mg specimens for fatigue test with Octet truss cell. The identification code of the specimens is: Cell shape-Cell size-Solid volume fraction (nominal)-Serial number.

Table A3. Octet Truss Fatigue Results.

Id Code	σ_M [MPa]	σ_m [MPa]	σ_a [MPa]	N
Oct-5-25-1	18.5	1.85	8.33	18,568
Oct-5-25-2	18.5	1.85	8.33	36,394
Oct-5-25-3	18.5	1.85	8.33	-
Oct-5-25-4	13.9	1.39	6.26	128,641
Oct-5-25-5	13.9	1.39	6.26	151,236
Oct-5-25-6	13.9	1.39	6.26	-
Oct-5-25-7	9.3	0.93	4.19	971,841
Oct-5-25-8	9.3	0.93	4.19	1,119,612
Oct-5-25-9	9.3	0.93	4.19	-
Oct-5-25-10	4.6	0.46	2.07	>15,000,000
Oct-5-25-11	4.6	0.46	2.07	15,000,000
Oct-5-25-12	4.6	0.46	2.07	-
Oct-5-30-1	22.7	2.27	10.22	64,099
Oct-5-30-2	22.7	2.27	10.22	52,684
Oct-5-30-3	22.7	2.27	10.22	-
Oct-5-30-4	17	1.7	7.65	239,878
Oct-5-30-5	17	1.7	7.65	234,151
Oct-5-30-6	17	1.7	7.65	-
Oct-5-30-7	11.3	1.13	5.09	880,174
Oct-5-30-8	11.3	1.13	5.09	645,908
Oct-5-30-9	11.3	1.13	5.09	-
Oct-5-30-10	5.7	0.57	2.57	>15,000,000
Oct-5-30-11	5.7	0.57	2.57	>15,000,000
Oct-5-30-12	5.7	0.57	2.57	-
Oct-7-30-1	22.9	2.29	10.31	10,607
Oct-7-30-2	22.9	2.29	10.31	9009
Oct-7-30-3	22.9	2.29	10.31	25,343
Oct-7-30-4	17.2	1.72	7.74	42,201
Oct-7-30-5	17.2	1.72	7.74	68,178
Oct-7-30-6	17.2	1.72	7.74	35,084
Oct-7-30-7	11.5	1.15	5.18	136,536
Oct-7-30-8	11.5	1.15	5.18	86,464
Oct-7-30-9	11.5	1.15	5.18	204,722
Oct-7-30-10	5.7	0.57	2.57	3,108,586
Oct-7-30-11	5.7	0.57	2.57	-
Oct-7-30-12	5.7	0.57	2.57	-

Appendix B

This section reports the quality analysis of the outcomes provided by the fatigue experiments.

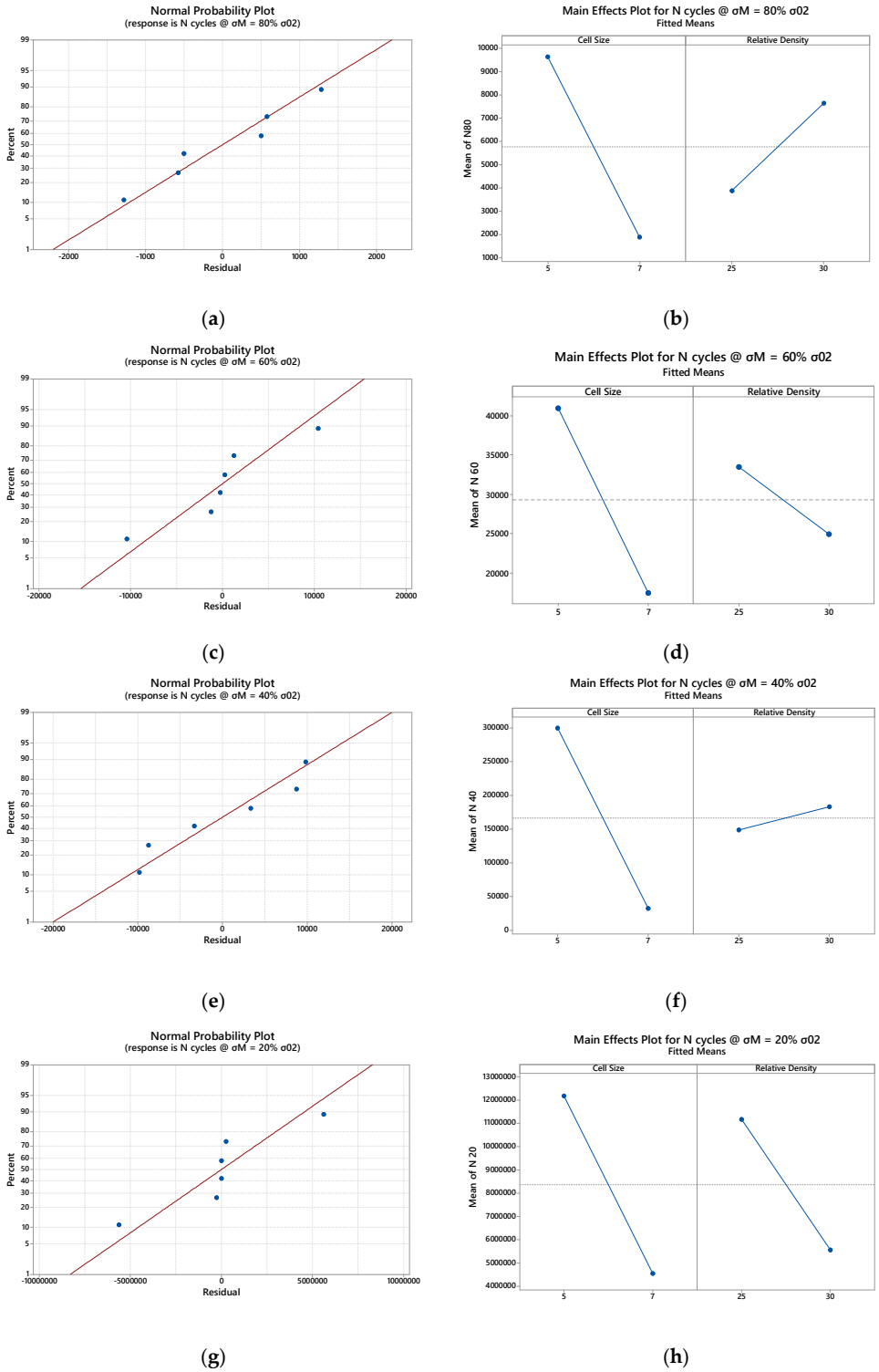

Figure A1. Rhombic Dodecahedron Cells Fatigue Outcome Statistical Analysis: (**a**) normal probability plot, max load 80% σ_{02}; (**b**) main effect plot, max load 80% σ_{02}; (**c**) normal probability plot, max load 60% σ_{02}; (**d**) main effect plot, max load 60% σ_{02}; (**e**) normal probability plot, max load 40% σ_{02}; (**f**) main effect plot, max load 40% σ_{02}; (**g**) normal probability plot, max load 20% σ_{02}; (**h**) main effect plot, max load 20% σ_{02}.

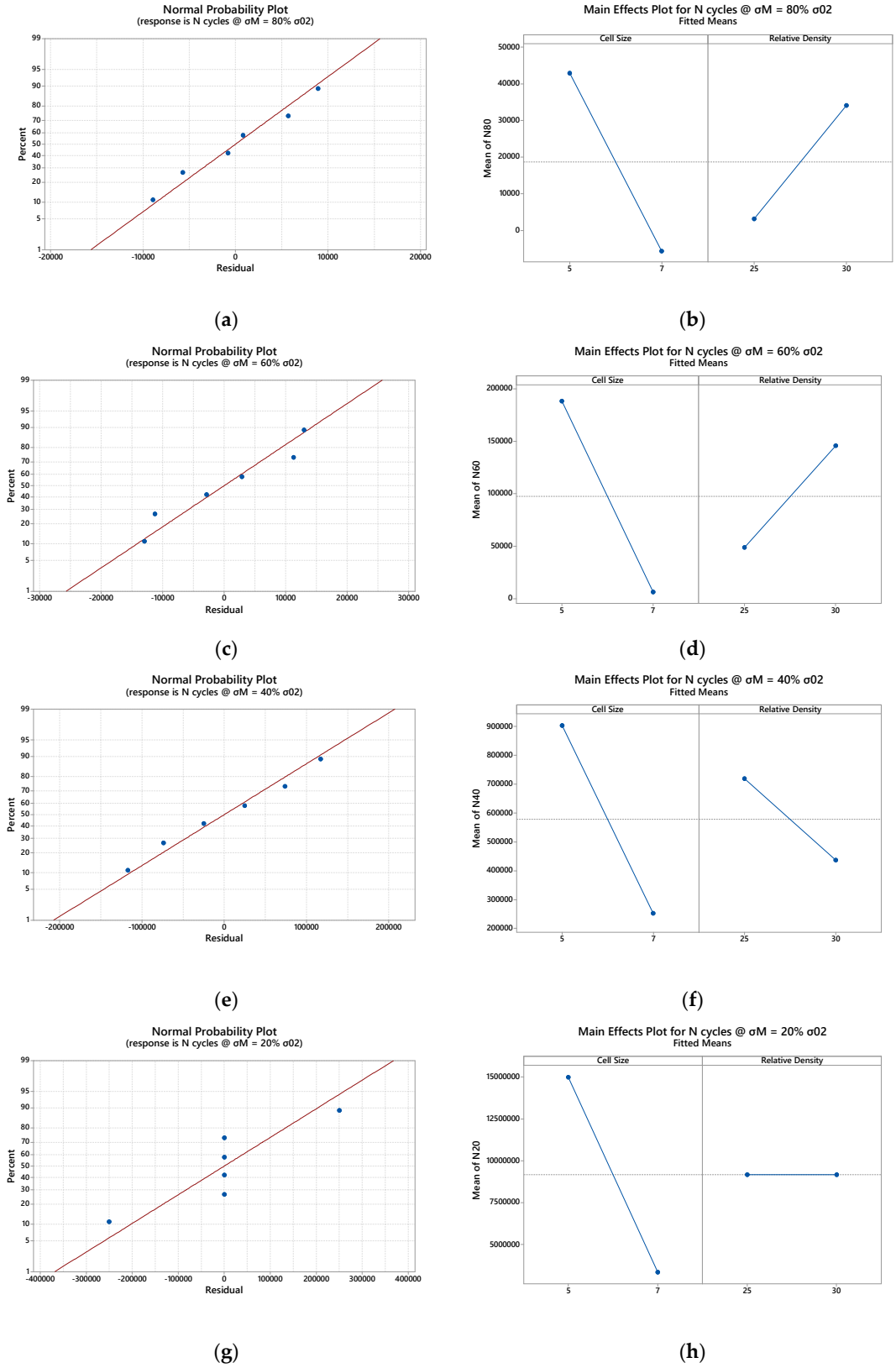

Figure A2. Octet Truss Cell Fatigue Outcome Statistical Analysis: (**a**) normal probability plot, max load 80% σ_{02}; (**b**) main effect plot, max load 80% σ_{02}; (**c**) normal probability plot, max load 60% σ_{02}; (**d**) main effect plot, max load 60% σ_{02}; (**e**) normal probability plot, max load 40% σ_{02}; (**f**) main effect plot, max load 40% σ_{02}; (**g**) normal probability plot, max load 20% σ_{02}; (**h**) main effect plot, max load 20% σ_{02}.

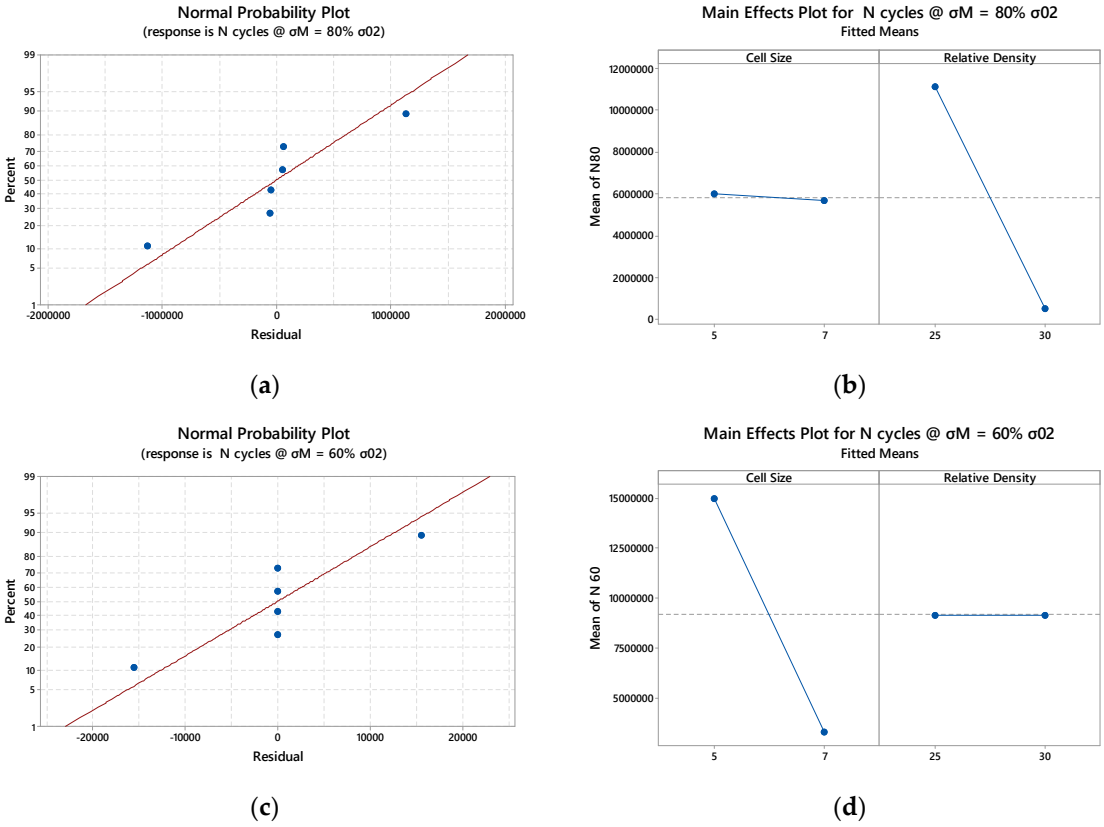

Figure A3. Bccz Truss Cells Fatigue Outcome Statistical Analysis: (**a**) normal probability plot, max load 80% σ_{02}; (**b**) main effect plot, max load 80% σ_{02}; (**c**) normal probability plot, max load 60% σ_{02}; (**d**) main effect plot, max load 60% σ_{02}.

Appendix C

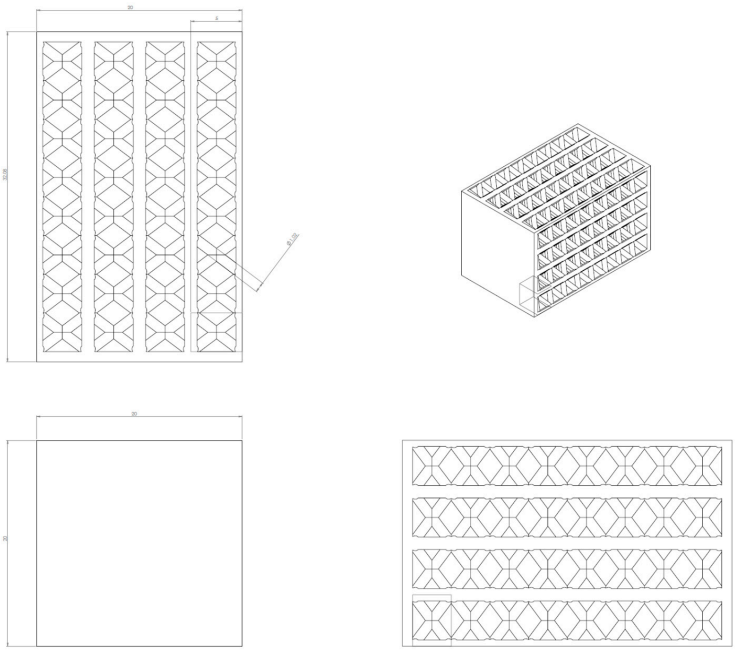

(**a**)

Figure A4. *Cont.*

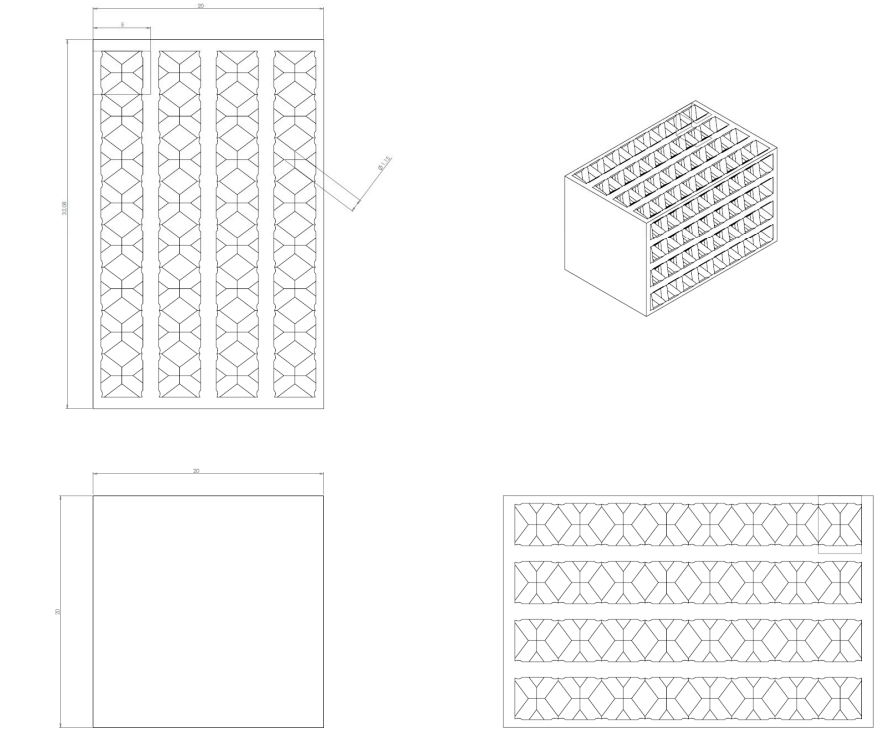

(**b**)

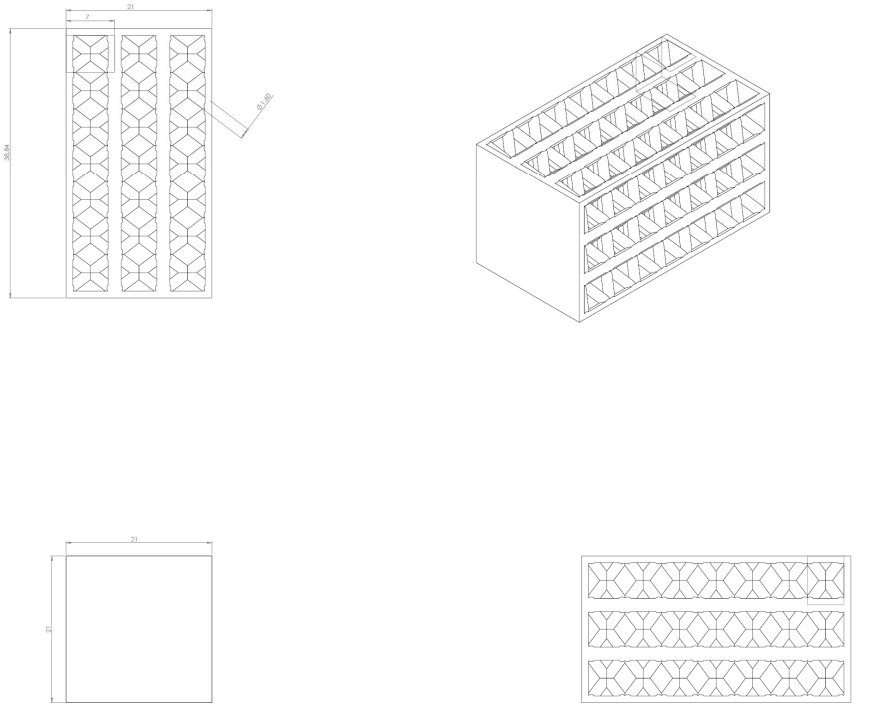

(**c**)

Figure A4. Bccz Cells Design: (**a**) 5 mm cells, 25% relative density; (**b**) 5 mm cells, 30% relative density; (**c**) 7 mm cells, 25% relative density.

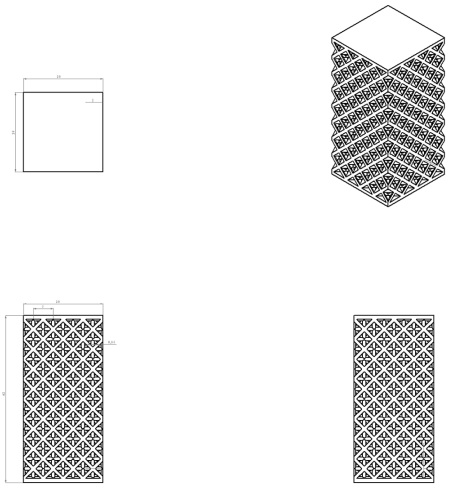

(**a**)

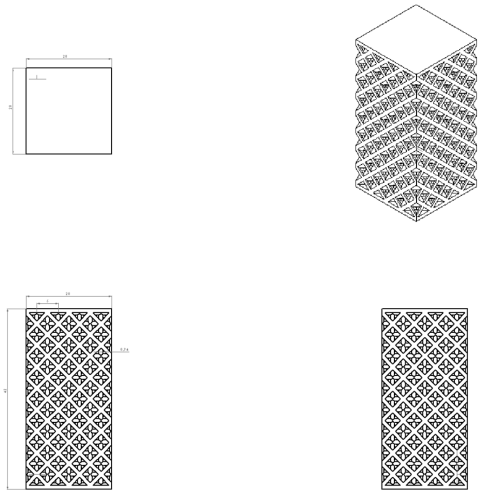

(**b**)

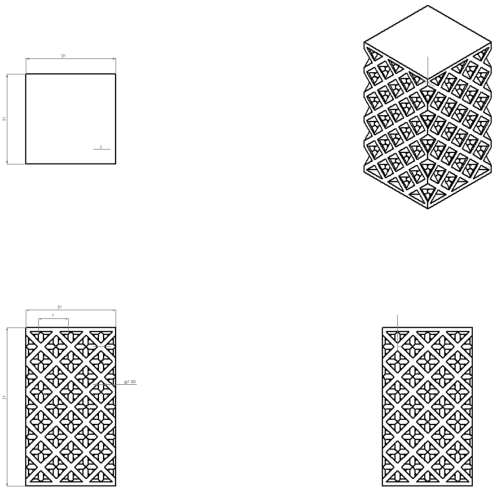

(**c**)

Figure A5. Octet Cells Design: (**a**) 5 mm cells, 25% relative density; (**b**) 5 mm cells, 30% relative density; (**c**) 7 mm cells, 25% relative density.

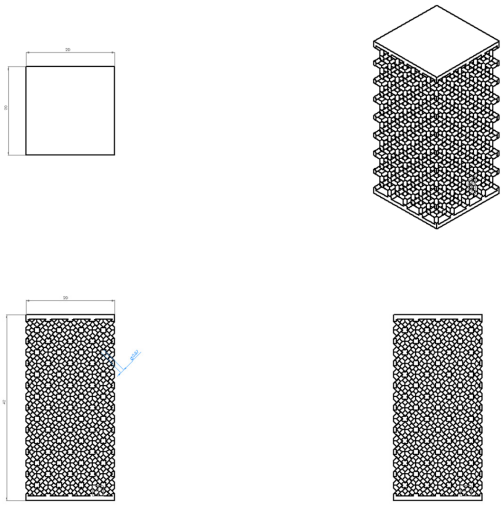

(**a**)

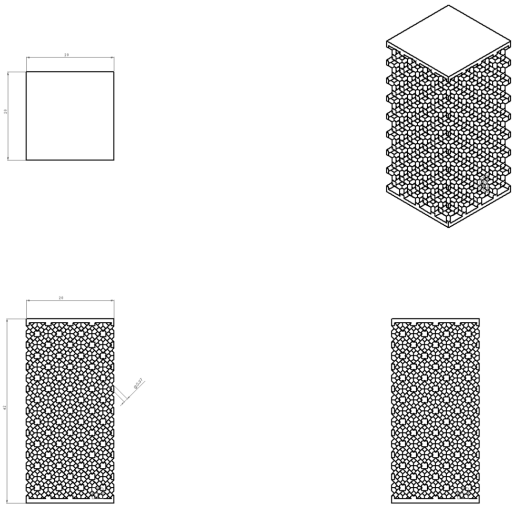

(**b**)

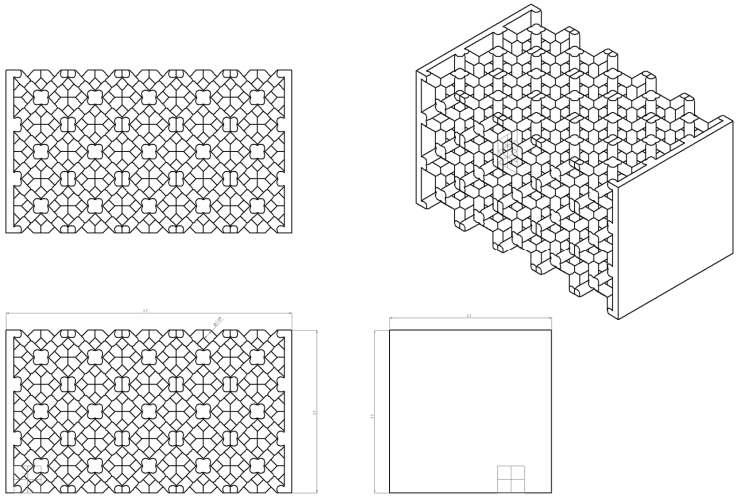

(**c**)

Figure A6. Rhombic Cells Design: (**a**) 5 mm cells, 25% relative density; (**b**) 5 mm cells, 30% relative density; (**c**) 7 mm cells, 25% relative density.

References

1. Ferro, C.; Grassi, R.; Seclì, C.; Maggiore, P. Additive Manufacturing Offers New Opportunities in UAV Research. *Procedia CIRP* **2016**, *41*, 1004–1010. [CrossRef]
2. Stornelli, G.; Gaggia, D.; Rallini, M.; Di Schino, A. Heat Treatment Effect on Maraging Steel Manufactured by Laser Powder Bed Fusion Technology: Microstructure and Mechanical Properties. *Acta Metall. Slovaca* **2021**, *27*, 122–126. [CrossRef]
3. Benedetti, M.; du Plessis, A.; Ritchie, R.; Dallago, M.; Razavi, S.; Berto, F. Architected cellular materials: A review on their mechanical properties towards fatigue-tolerant design and fabrication. *Mater. Sci. Eng. R Rep.* **2021**, *144*, 100606. [CrossRef]
4. Blakey-Milner, B.; Gradl, P.; Snedden, G.; Brooks, M.; Pitot, J.; Lopez, E.; Leary, M.; Berto, F.; du Plessis, A. Metal additive manufacturing in aerospace: A review. *Mater. Des.* **2021**, *209*, 110008. [CrossRef]
5. Korkmaz, M.E.; Gupta, M.K.; Robak, G.; Moj, K.; Krolczyk, G.M.; Kuntoğlu, M. Development of lattice structure with selective laser melting process: A state of the art on properties, future trends and challenges. *J. Manuf. Process.* **2022**, *81*, 1040–1063. [CrossRef]
6. Cao, Y.; Tan, W.; Wu, Z. Aircraft icing: An ongoing threat to aviation safety. *Aerosp. Sci. Technol.* **2018**, *75*, 353–385. [CrossRef]
7. Ferro, C.G.; Varetti, S.; Maggiore, P.; Lombardi, M.; Biamino, S.; Manfredi, D.; Calignano, F. Design and characterization of trabecular structures for an anti-icing sandwich panel produced by additive manufacturing. *J. Sandw. Struct. Mater.* **2020**, *22*, 1111–1131. [CrossRef]
8. Maggiore, P.; Vitti, F.; Ferro, C.G.; Sara, V. Thermal Anti Ice System Integrated in the Structure and Method for Its Fabrication. U.S. Patent 102016000098196, 2016.
9. Goraj, Z. An Overview of the Deicing and Anti-Icing Technologies with Prospects for the Future. In Proceedings of the 24th International Congress of the Aeronautical Sciences, Yokohama, Japan, 29 August–3 September 2004.
10. Pellissier, M.P.C.; Habashi, W.G.; Pueyo, A. Optimization via FENSAP-ICE of aircraft hot-air anti-icing systems. *J. Aircr.* **2011**, *48*, 265–276. [CrossRef]
11. Al-Khalil, K.M.; Keith, T.G.; DeWitt, K.J.; Nathman, J.K.; Dietrich, D.A. Thermal analysis of engine inlet anti-icing systems. *J. Propuls. Power* **1990**, *6*, 628–634. [CrossRef]
12. Papadakis, M.; Wong, S.-H.; Yeong, H.-W.; Vu, G. Icing Tunnel Experiments with a Hot Air Anti-Icing System. In Proceedings of the 46th AIAA Aerospace Sciences Meeting and Exhibit, Reno, NV, USA, 7–10 January 2008. [CrossRef]
13. Morency, F.; Tezok, F.; Paraschivoiu, I. Heat and mass transfer in the case of anti-icing system simulation. *J. Aircr.* **2000**, *37*, 245–252. [CrossRef]
14. Manogharan, G. *Analysis of Non-Stochastic Lattice Structure Design for Heat Exchanger*; NC State University: Raleigh, NC, USA, 2009.
15. Tancogne-Dejean, T.; Spierings, A.B.; Mohr, D. Additively-manufactured metallic micro-lattice materials for high specific energy absorption under static and dynamic loading. *Acta Mater.* **2016**, *116*, 14–28. [CrossRef]
16. Hao, L.; Raymont, D.; Yan, C.; Hussein, A.; Young, P. Design and Additive Manufacturing of Cellular Lattice Structures. In Proceedings of the The International Conference on Advanced Research in Virtual and Rapid Prototyping (VRAP), Leiria, Portugal, 28 September–1 October 2011; pp. 249–254. [CrossRef]
17. Zargarian, A.; Esfahanian, M.; Kadkhodapour, J.; Ziaei-Rad, S.; Zamani, D. On the fatigue behavior of additive manufactured lattice structures. *Theor. Appl. Fract. Mech.* **2019**, *100*, 225–232. [CrossRef]
18. Burr, A.; Persenot, T.; Doutre, P.-T.; Buffiere, J.-Y.; Lhuissier, P.; Martin, G.; Dendievel, R. A numerical framework to predict the fatigue life of lattice structures built by additive manufacturing. *Int. J. Fatigue* **2020**, *139*, 105769. [CrossRef]
19. Agenbag, N.; McDuling, C. Fatigue Life Testing of Locally Additive Manufactured AlSilOMg Test Specimens. *R&D J.* **2021**, *37*, 19–25. [CrossRef]
20. Tommasi, A.; Maillol, N.; Bertinetti, A.; Penchev, P.; Bajolet, J.; Gili, F.; Pullini, D.; Mataix, D.B. Influence of surface preparation and heat treatment on mechanical behavior of hybrid aluminum parts manufactured by a combination of laser powder bed fusion and conventional manufacturing processes. *Metals* **2021**, *11*, 522. [CrossRef]
21. Bici, M.; Brischetto, S.; Campana, F.; Ferro, C.G.; Seclì, C.; Varetti, S.; Maggiore, P.; Mazza, A. Development of a multifunctional panel for aerospace use through SLM additive manufacturing. *Procedia CIRP* **2018**, *67*, 215–220. [CrossRef]
22. Yan, C.; Hao, L.; Hussein, A.; Bubb, S.L.; Young, P.; Raymont, D. Evaluation of light-weight AlSi10Mg periodic cellular lattice structures fabricated via direct metal laser sintering. *J. Mater. Process. Technol.* **2014**, *214*, 856–864. [CrossRef]
23. Perello, M. Numerical Simulation and Experimental Validation of Lattice Structures for an Innovative Anti-Ice Leading Edge. 2018. Available online: http://webthesis.biblio.polito.it/id/eprint/9219 (accessed on 1 March 2023).
24. Hussein, A.; Hao, L.; Yan, C.; Everson, R.; Young, P. Advanced lattice support structures for metal additive manufacturing. *J. Mater. Process. Technol.* **2013**, *213*, 1019–1026. [CrossRef]
25. Maconachie, T.; Leary, M.; Lozanovski, B.; Zhang, X.; Qian, M.; Faruque, O.; Brandt, M. SLM lattice structures: Properties, performance, applications and challenges. *Mater. Des.* **2019**, *183*, 108137. [CrossRef]
26. du Plessis, A.; Razavi, S.M.J.; Benedetti, M.; Murchio, S.; Leary, M.; Watson, M.; Bhate, D.; Berto, F. Properties and applications of additively manufactured metallic cellular materials: A review. *Prog. Mater. Sci.* **2022**, *125*, 10918. [CrossRef]
27. Seharing, A.; Azman, A.H.; Abdullah, S. A review on integration of lightweight gradient lattice structures in additive manufacturing parts. *Adv. Mech. Eng.* **2020**, *12*, 1687814020916951. [CrossRef]

28. Mahmoud, D.; Elbestawi, M.A. Elbestawi, Lattice structures and functionally graded materials applications in additive manufacturing of orthopedic implants: A review. *J. Manuf. Mater. Process.* **2017**, *1*, 13. [CrossRef]
29. Muhammad, M.; Nezhadfar, P.; Thompson, S.; Saharan, A.; Phan, N.; Shamsaei, N. A comparative investigation on the microstructure and mechanical properties of additively manufactured aluminum alloys. *Int. J. Fatigue* **2021**, *146*, 106165. [CrossRef]
30. Ferro, C.G.; Varetti, S.; Vitti, F.; Maggiore, P.; Lombardi, M.; Biamino, S.; Manfredi, D.; Calignano, F. A robust multifunctional sandwich panel design with trabecular structures by the use ofadditive manufacturing technology for a new de-icing system. *Technologies* **2017**, *5*, 35. [CrossRef]
31. Zilio, C.; Patricelli, L. Aircraft anti-ice system: Evaluation of system performance with a new time dependent mathematical model. *Appl. Therm. Eng.* **2014**, *63*, 40–51. [CrossRef]
32. Montgomery, D.C. *Design and Analysis of Experiments*; John Wiley & Sons, Inc.: Scottsdale, AZ, USA, 2019; p. 684.
33. Lambert, D.; Adler, M. IN718 Additive Manufacturing Properties and Influences. In Proceedings of the JANNAF Propulsion Meeting, Nashville, TN, USA, 1–4 June 2014.
34. McCullough, K.Y.G.; Fleck, N.A.; Ashby, M.F. Stress-life fatigue behaviour of aluminum alloy foams. *Fatigue Fract. Eng. Mater. Struct.* **2000**, *23*, 199–208. [CrossRef]
35. Zhao, S.; Li, S.; Hou, W.; Hao, Y.; Yang, R.; Misra, R. The influence of cell morphology on the compressive fatigue behavior of Ti-6Al-4V meshes fabricated by electron beam melting. *J. Mech. Behav. Biomed. Mater.* **2016**, *59*, 251–264. [CrossRef] [PubMed]
36. Zenkert, D.; Burman, M. Tension, compression and shear fatigue of a closed cell polymer foam. *Compos. Sci. Technol.* **2009**, *69*, 785–792. [CrossRef]
37. Zhai, Y.; Galarraga, H.; Lados, D.A. Microstructure, static properties, and fatigue crack growth mechanisms in Ti-6Al-4V fabricated by additive manufacturing: LENS and EBM. *Eng. Fail. Anal.* **2016**, *69*, 3–14. [CrossRef]
38. Varetti, S. *Study and Development of an Innovative L-PBF Demonstrator and an Anti-Ice Solution Based on Trabecular Structures*; Politecnico di Torino: Turin, Italy, 2020.
39. Lazzeri, R. A comparison between safe life, damage tolerance and probabilistic approaches to aircraft structure fatigue design. *Aerotec. Missili Spaz.* **2002**, *81*.
40. Li, Y.; Pavier, M.; Coules, H. Compressive fatigue characteristics of octet-truss lattices in different orientations. *Mech. Adv. Mater. Struct.* **2022**, *29*, 6390–6402. [CrossRef]
41. Li, Y.; Pavier, M.; Coules, H. Experimental study on fatigue crack propagation of octet-truss lattice. *Procedia Struct. Integr.* **2021**, *37*, 41–48. [CrossRef]
42. Ashby, M.F. The properties of foams and lattices. *Philos. Trans. R. Soc. A Math. Phys. Eng. Sci.* **2006**, *364*, 15–30. [CrossRef] [PubMed]